The Catalytic Effect of Dihydrofolate Reductase and Its Mutants Is Determined by Reorganization Energies†

Hanbin Liu and Arieh Warshel*

Department of Chemistry, University of Southern California, 3620 McClintock Avenue, Los Angeles, California 90089-1062

Received January 30, 2007; Revised Manuscript Received March 8, 2007

ABSTRACT: The effect of distant mutations on the catalytic reaction of dihydrofolate reductase (DHFR) is reexamined by empirical valence bond simulations. The simulations reproduce for the first time the changes in the observed rate constants (without the use of adjustable parameters for this purpose) and show that the changes in activation barriers are strongly correlated with the corresponding changes in the reorganization energy. The preorganization of the polar groups of enzymes is the key catalytic factor, and anticatalytic mutations destroy this preorganization. Some anticatalytic mutations in DHFR also increase the distance between the donor and acceptor, but this effect is not directly related to catalysis since the native enzyme and the uncatalyzed reaction in water have similar average donor−acceptor distances. Insight into the effect of a mutation is provided by constructing the relevant free energy surfaces in terms of the generalized solute−solvent coordinates. It is shown how the mutations change the reaction coordinate and the activation barrier, and it is clarified that the corresponding changes do not reflect dynamical effects. It is also pointed out that all reactions in a condensed phase involve correlated motions (both in enzymes and in solution) and that the change of such motions upon mutations is a result of the change in the shape of the multidimensional reaction path on the solute−solvent surface, rather than the reason for the change in rate constant. Thus, as far as catalysis is concerned, the change in the activation barrier is due to the change in the electrostatic preorganization energy.

Enzymes play fundamental roles in almost all life processes. They accelerate a great variety of metabolic reactions and control such processes as signaling, energy transduction, and translation of genetic information. Their ability to catalyze reactions by many orders of magnitude allows cells to carry out reactions that otherwise would not occur on biologically useful time scales. There is, therefore, broad interest in understanding the origin of this catalytic power on a molecular level. Although it is clear that electrostatic effects play a major role in stabilizing the transition states of enzymatic reactions (for review see ref *1*), it is important to explore the importance of other factors. In particular, there is great current interest in dynamical effects and correlated motions (*2*−*6*) and in the idea that such motions play a major role in catalysis. One of the systems that have drawn the largest attention as a benchmark for dynamical contributions to catalysis is the enzyme dihydrofolate reductase (DHFR).

Benkovic, Wright, and co-workers (*2*, *3*, *7*−*9*) have studied the reaction of dihydrofolate reductase by NMR. They found that site-directed mutations of residues in a loop that undergoes relatively large backbone motions had detrimental effects on catalysis, and they suggested that the dynamics of these residues could be important for catalysis. Brooks and co-workers (*10*, *11*) carried out MD simulations of three ternary complexes of the enzyme and found that motions of some residues were strongly correlated, and were different in the enzyme−substrate (ES) and enzyme−product (EP) complexes. The simulated motions in mutant enzymes with diminished activity were considered as supporting the dynamical proposal. However, these studies did not examine the transition states in the reaction or demonstrate any dynamical effects on the rate constant. The different motions of the ES and EP complexes could just reflect the coupling of enzyme−substrate interactions to interactions of various groups in the protein, which is common to all enzymes. Hammes-Schiffer, Benkovic, and their co-workers (*4*, *11*, *12*), who evaluated the actual activation barrier, identified a network of correlated conformational changes with projections on the reaction path, but concluded that these reflect equilibrium structural effects rather than dynamical effects. QM/MM simulations described by Garcia-Vilocoa et al. (*13*) and by Thorpe and Brooks (*14*) also appear to be in accord with this view.

The idea that correlated motions play an important role in catalysis is not without problems since (see ref *5*) correlated motions exist in all reactions in condensed phases. Here it is important to identify the actual factors that control the difference between the rates of the reaction in the enzyme and in solution as well as the difference between the native and mutated enzymes. It seems likely that the key catalytic factor in DHFR is the electrostatic preorganization effect, as is the case with other enzymes (e.g., see ref *1*), and that the change in correlated motions upon mutations simply reflects the corresponding change in the reaction coordinate. However, the idea that dynamical effects play a major role in the catalytic reaction of DHFR remains a prominent

† This work was supported by Grant GM024492 from the National Institutes of Health (NIH).

* Corresponding author. E-mail: warshel@usc.edu. Phone: 213-740-4114. Fax: 213-740-2701.

10.1021/bi700201w CCC: $37.00 © 2007 American Chemical Society
Published on Web 05/01/2007

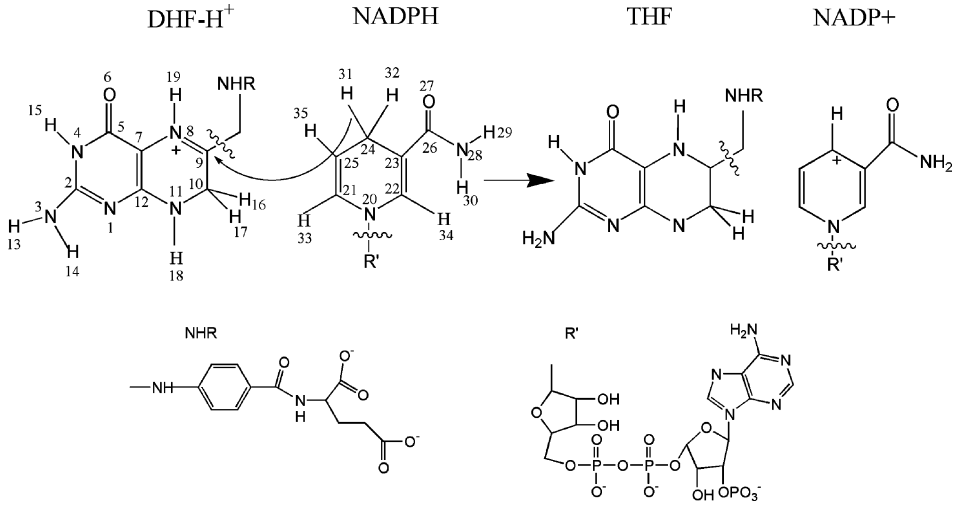

FIGURE 1: The reacting system in the catalytic reaction of DHFR. The EVB atoms are labeled by numbers that are used to define the EVB parameters in Tables S1 and S2 of the Supporting Information.

proposal as is evident from the very recent work of Boehr et al. (*15*) Apparently the meaning of dynamical contribution to catalysis depends on the definition (see ref *5*), but it is clear that many workers implied that dynamical effects are associated with non-Boltzmann fluctuation that presumably contributes to catalysis (see discussion in ref *5*). This is clearly implied by works that focused on having protein motions at a specific time scale and by the references quoted as the origin of the dynamical idea (typically refs *16*−*18*, which proposed the equivalent of coherent motions). However, it is hard to find compelling support of this view in the currently available theoretical and experimental studies (see ref *5* for a discussion), and indeed many current works argue now that what is meant by dynamical effect is the availability of many structures in equilibrium processes and of any motion, regardless if it is thermal motion or not (e.g., ref *19*). Thus this paper is not about what is meant by the dynamical proposals (a subject which is very important in our view (see ref *5*) but about the idea that correlated motion has special catalytic significance.

The present work will reexamine the origin of the catalytic effect in DHFR and the role of distant mutations. Our study will start by reproducing the effects of different mutations. This will allow us to explore in a quantitative way the factors that lead the change in the corresponding rate constants. It will be shown that the main effects of the mutations are associated with the change of the reorganization energy. Decomposing these changes to solute and solvent contributions will allow us to describe the change in the reaction coordinate and to clarify the relationship between mutational alosteric effects and the reduction in the catalytic power of the enzyme. We will also consider an alternative decomposition to work term and solvent reorganization energy that will provide a useful way of handling the effect of the protein on the donor−acceptor distance.

METHODS

The main challenge of the present work is the evaluation of the effect of distant mutations in a sufficiently reliable way to allow for a meaningful analysis of the origin of the catalytic effect. This requires very extensive sampling, which

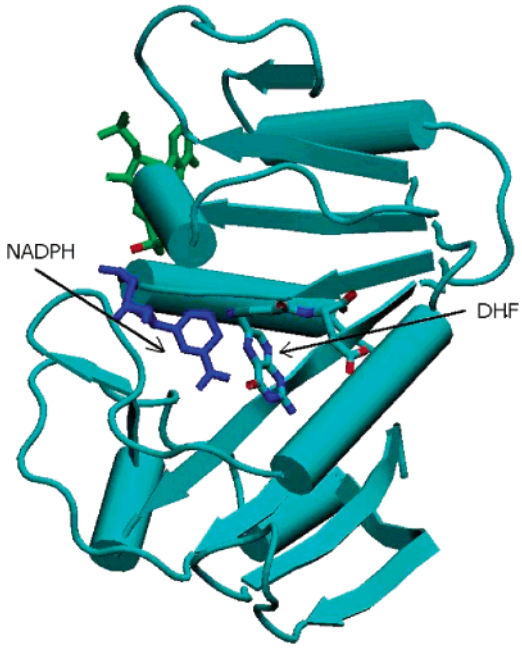

FIGURE 2: Showing the overall structure of DHFR and the location of the reacting system. The structure was generated by using the VMD program (*92*).

is hard to accomplish reliably by current molecular orbital QM/MM methods despite significant advances in this direction in studies of different enzymes in general (for review see ref *20*) and DHFR in particular (e.g., refs *13*, *14*, *21*, *22*). We believe that at present the most effective strategy is to use the empirical valence bond (EVB[1]) method (e.g., refs *1* and *23*). This is particularly important in view of the need to evaluate the reorganization energies. Thus we use the EVB here as our main simulation tool. This method has been described extensively elsewhere (e.g., refs *1* and *23*), and only some key details are given here.

The reacting system is described schematically in Figure 1, and the location of the reactants in DHFR is depicted in Figure 2. This system is represented by the two diabatic states

[1] Abbreviations: EVB, empirical valence bond; FEP, free energy perturbation; US, umbrella sampling; NQM, nuclear quantum mechanical.

$$\Psi_1 = \mathrm{D{-}H}\quad \mathrm{A^+}$$
$$\Psi_2 = \mathrm{D^+\ H{-}A} \qquad (1)$$

where DH, D^+, A^+, and AH are the NADPH, $NADP^+$, $DHF-H^+$, and THF systems described in Figure 1.

The potential energies of these states (H_{11} and H_{22}) and the mixing term (H_{12}) are represented by the Hamiltonian matrix elements

$$H_{ii} = \epsilon_i = \alpha^{\mathrm{i}}_{\mathrm{gas}} + U^{\mathrm{i}}_{\mathrm{intra}}(\boldsymbol{R}) + U^{\mathrm{i}}_{\mathrm{inter}}(\boldsymbol{R},\boldsymbol{r}) + U^{\mathrm{i}}_{\mathrm{solvent}}(\boldsymbol{r}) \quad (2a)$$

$$H_{ij} = A\left(\frac{1}{1+\mathrm{e}^{-B((\epsilon_j-\epsilon_i)+C)}} + \frac{1}{1+\mathrm{e}^{B((\epsilon_j-\epsilon_i)-C)}} + 1\right) \times \exp\{-\mu R\} \quad (2b)$$

Here $\boldsymbol{R}$ is the vector of the atomic coordinates of the reactants or products ("solute") in the diabatic states, and $\boldsymbol{r}$ is the vector of atomic coordinates of the surrounding water or protein ("solvent"). $\alpha^{\mathrm{i}}_{\mathrm{gas}}$ is the energy of the ith diabatic state in the gas phase, where all the fragments are at infinite separation; $U^{\mathrm{i}}_{\mathrm{intra}}(\boldsymbol{R})$ is the intramolecular potential of the solute system (relative to its minimum) in this state; $U^{\mathrm{i}}_{\mathrm{inter}}(\boldsymbol{R},\boldsymbol{r})$ represents the interaction between the solute atoms and the surrounding solvent atoms; and $U^{\mathrm{i}}_{\mathrm{solvent}}(\boldsymbol{r})$ represents the potential energy of the solvent.

The ϵ_i given by eq 2a form the diagonal elements (H_{ii}) of the EVB Hamiltonian (H_{EVB}). The off-diagonal elements of the Hamiltonian (H_{ij}) either are assumed to be constant or are represented by a function of the distances between the reacting atoms or the energy gap. In the present case we express H_{ij} as a function of the energy gap ($\epsilon_j - \epsilon_i$) between the diabatic reactant and product states and use the parameters A, B, and C, which are adjusted to fit either quantum calculations or experiment. The H_{ij} elements are assumed to be the same in the gas phase, in solution, and in the protein. This important assumption has been recently shown to provide quite a good approximation for the corresponding *ab initio* results (*24*) for charge-transfer reactions in the gas phase and in solution (*24*) (see also ref *25*). Furthermore, this assumption is consistent with observed linear free energy relationships (see discussion in ref *24*) and is very reasonable when one compares different mutants of the same enzyme. The adiabatic ground-state energy (E_{g}) and the corresponding eigenvector (C_{g}) are obtained by solving the secular equation

$$\boldsymbol{H}_{\mathrm{EVB}}\boldsymbol{C}_{\mathrm{g}} = E_{\mathrm{g}}\boldsymbol{C}_{\mathrm{g}} \qquad (3)$$

The simplicity of the EVB formulation makes it relatively straightforward to obtain analytical derivatives of the potential surface by using the Hellmann−Feynman theorem for eq 3, and thus to sample the EVB energy surface by molecular-dynamics (MD) simulations. In principle, running MD trajectories on the EVB surface of the reactant state can provide the free energy profile $\Delta g(x')$ (where x' is the reaction coordinate) that is needed to calculate the activation free energy ($\Delta g^{\ddagger}$).

The details of the mapping procedure used to evaluate the EVB free energy surface are described elsewhere (*23*, *26*), and here we review here only essential points for the simple case of two diabatic states. In such a case we use a mapping potential of the form

$$\epsilon_m = (1-\theta_m)\epsilon_1 + \theta_m\epsilon_2 \qquad (4)$$

where θ_m changes from 0 to 1 in $n+1$ fixed increments ($\theta_m = 0/n, 1/n, 2/n, ..., n/n$). The free energy ΔG_m associated with changing λ from 0 to m/n can be evaluated by a free energy perturbation (FEP) procedure. The free energy functional that corresponds to the adiabatic ground state surface, E_{g} is obtained by the FEP−umbrella sampling (FEP/US) method, which can be written as

$$\Delta g(x') = \Delta G_m - \beta^{-1}\ln\langle\delta(x-x')\times \exp\{-\beta[E_{\mathrm{g}}(x) - \epsilon_m(x)]\}\rangle_m \quad (5)$$

In this expression, ϵ_m is the mapping potential that keeps the reaction coordinate x in the region of x', $\langle\cdots\rangle_m$ denotes an average over an MD trajectory on this potential, $\beta = (k_{\mathrm{B}}T)^{-1}$, k_{B} is the Boltzmann constant, and T is the temperature. If the changes in ϵ_m are sufficiently gradual, the free energy profile $\Delta g(x')$ obtained with several values of m overlap over a range of x', and patching together the full set of $\Delta g(x')$ gives a complete free energy curve for the reaction.

The FEP/US approach also can be used to obtain the free energy functional of the individual diabatic states. For example, the free energy functional of the reactant state (Δg_1) is

$$\Delta g_1(x') = \Delta G_m - \beta^{-1}\ln\langle\delta(x-x')\times \exp\{-\beta[\epsilon_1(x) - \epsilon_m(x)]\}\rangle_m \quad (6)$$

The diabatic free energy profiles of the reactant and product states represent microscopic equivalents of the Marcus parabolas in electron-transfer theory (*27*) and can be used to obtain the microscopic reorganization energy.

In order to relate the origin of the catalytic effect to the EVB results, it is convenient to approximate the activation free energy by the modified Marcus equation (*23*, *28*):

$$\Delta g^{\ddagger} = \bar{w} + ((\Delta G^0)' + \lambda)^2/4\lambda - \bar{H}_{12}(x) + \frac{\bar{H}_{12}(R_0)}{((\Delta G^0)' + \lambda)} - \Gamma \quad (7)$$

where $\bar{w}$ is the so-called "work term" that describes the free energy of bringing the donor and acceptor to the interaction distance (R_0) at the reactant state, λ is the reorganization energy, $(\Delta G^0)'$ is the diabatic reaction free energy, Γ is the nuclear quantum mechanical correction, and the $\bar{H}_{12}$ are the average values of H_{12} in the TS ($x^{\ddagger}$) and the reactant state (x_0). The nature of this expression is defined schematically in Figure 3 in the case of a fixed donor and acceptor distance (where the $\bar{w}$ term is not needed). The first two terms of eq 7 are those used in Marcus formulation for electron-transfer reactions (*27*), and the rest of the expression represents the effect of the very strong mixing (H_{12}) between the diabatic states. The second term reflects the reduction of the energy at the adiabatic ground state at the TS relative to the diabatic energy due to H_{12}. The third term represents the reduction of the energy of the adiabatic ground state at the reactant region due to the effect of H_{12}. The crucial role of the mixing term has been discussed and demonstrated previously (e.g., ref *29*). The reorganization energy can be obtained directly from the EVB diabatic free energies as will be discussed below.

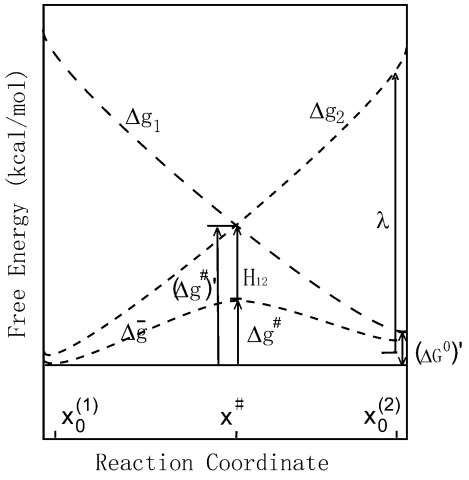

FIGURE 3: Demonstrating the relationship between the diabatic surfaces (Δg_i) and adiabatic surfaces ($\Delta \bar{g}$) in the EVB treatment. The figure demonstrates the effect of the mixing term H_{12} (changing the diabatic barrier, $(\Delta g^{\ddagger})'$, to the adiabatic barrier, $\Delta g^{\ddagger}$) and defines the reorganization energy, λ.

Since we are interested in mode coupling, it is important to clarify the actual effect of the mutations on the reaction coordinate and the potential surface for the hydride transfer reaction. One way to explore this issue is to describe the potential surface in terms of the solute and solvent coordinates. This is done by expressing the quasiharmonic approximation of the EVB states (*26*):

$$\begin{aligned}\epsilon_1 &\cong \sum_i \frac{\hbar}{2}\omega_r^i\left(r_i + \frac{\Delta_r^i}{2}\right)^2 + \sum_j \frac{\hbar}{2}\omega_q^j\left(q_j + \frac{\Delta_q^j}{2}\right)^2 \\ &\cong \frac{\hbar}{2}\omega_R^i\left(R + \frac{\Delta_R}{2}\right)^2 + \frac{\hbar}{2}\omega_Q^i\left(Q + \frac{\Delta_Q}{2}\right)^2 \\ \epsilon_2 &\cong \sum_i \frac{\hbar}{2}\omega_r^i\left(r_i - \frac{\Delta_r^i}{2}\right)^2 + \sum_j \frac{\hbar}{2}\omega_q^j\left(q_j - \frac{\Delta_q^j}{2}\right)^2 + \Delta V_0 \\ &\cong \frac{\hbar}{2}\omega_R^i\left(R - \frac{\Delta_R}{2}\right)^2 + \frac{\hbar}{2}\omega_Q^i\left(Q - \frac{\Delta_Q}{2}\right)^2 + \Delta V_0 \quad (8)\end{aligned}$$

where R and Q are the effective dimensionless coordinates for the solute and solvent respectively. The effective frequencies ω_Q and ω_R are evaluated by $\omega = \int \omega P(\omega)\, d\omega$ in which $P(\omega)$ is the normalized power spectrum of the corresponding contribution to $(\epsilon_2 - \epsilon_1)$. The R are related to the regular reaction coordinate $R' = (b_1 - b_2)$ by $R = R'(\omega_R \mu_R/\hbar)^{1/2}$, where μ_R is the reduced mass for the normal mode that is the compression of b_1 and extension of b_2. The reaction coordinate Q is defined in terms of the electrostatic contribution $(\epsilon_2 - \epsilon_1)_{el}$ to $(\epsilon_2 - \epsilon_1)$. Thus, we have $Q = (2(\epsilon_2 - \epsilon_1)_{el}/\hbar\omega_Q)^{1/2}$, which is also related to the regular solvent coordinate, Q', by $Q = Q'(\omega_Q m_Q/\hbar)^{1/2}$. ΔV_0 is the difference between the minima of ϵ_2 and ϵ_1. Here we replace the contribution from each set of coordinates by one effective coordinate. The displacement Δ's are related to the so-called reorganization energy, λ, given by

$$\lambda = \lambda_R + \lambda_Q = \sum_i (\hbar/2)\omega_r^i(\Delta_r^i)^2 + \sum_j (\hbar/2)\omega_q^j(\Delta_q^j)^2 \cong (\hbar/2)\omega_R\Delta_R^2 + (\hbar/2)\omega_Q\Delta_Q^2 \quad (9)$$

The EVB/US simulations were performed with the MOLARIS simulation program (*30*) using the ENZYMIX force field. Following the standard MOLARIS protocol we divided the simulation system into four regions. Region I included the folate and the NADPH (see Figure 1); region II included the protein plus the water molecules in and around protein up to a radius of 20 Å; region III included protein atoms and water molecules that were subjected to distance and polarization constraints according to the surface constrained all atom solvent (SCAAS) boundary condition (*31*). The rest of the system was represented by a bulk region with a dielectric constant of 80. The long-range electrostatic effects were treated by the local reaction field (LRF) method (*32*) that provides one of the most rigorous ways of treating electrostatic effects in protein and other nonperiodic systems. We also would like to point out that the SCAAS+LRF treatment were subjected to very extensive validation studies, in terms of the insensitivity of the calculated electrostatic free energy to changes in the size of the system (e.g., refs *33*−*35*). We are not aware of reported studies of this type for other approaches.

The charges of the EVB states were obtained by using the Gaussian03 package (*36*). This was done by optimizing the structures of the reactant and product in the gas phase using B3LYP (*37*, *38*) with the 6-31+g(d) basis set (*39*, *40*) and solvating the resulting structures in the PCM solvent model (*41*, *42*) using the 6-31g(d) (*39*) basis set. The resulting solvated PCM charges are summarized in Table S1 of the Supporting Information. The remaining EVB parameters of the solute system were obtained by fitting the EVB surface of the reacting system to the general feature at a consensus surface that reflects *ab initio* calculations and the experimental results which are discussed in the next section (the surface for the solution reaction in a solvent cage has been evaluated by the *ab initio* calculations described in S4, Supporting Information). As discussed in the next section we absorbed the nuclear quantum mechanical corrections in the classical EVB surface (see also ref *28*). The EVB parameters are given in Table S2 of the Supporting Information. The nonreacting part of the EVB surface was described by the ENZYMIX force field (*30*). The DHF system in the reactant states was assumed to be protonated in view of the considerations of previous studies (*43*−*45*) (see discussion in the next section).

The evaluation of the free energy profile involved the following procedure: the simulation system was equilibrated and relaxed for 300 ps, and the relaxed system was then used in an EVB/US simulation. The simulations involved the use of the mapping potential of eq 4 in 31 "frames" (i.e., 31 values of θ_m in the EVB mapping of eq 4). Each frame was simulated for 180 ps with a time step of 1 fs at 300 K. A procedure similar to the replica exchange (parallel tempering) (*46*, *47*) approach was used in order to avoid getting trapped in unphysical configurations and to get better statistics. That is, once every 30 ps we exchanged the system at adjacent frames. On odd swap cycles, the exchanges were made on (θ_1, θ_2) (θ_3, θ_4) ... (θ_{29}, θ_{30}) frames. On even swap cycles, the exchanges were made on (θ_2, θ_3) (θ_4, θ_5) ... (θ_{30}, θ_{31}) frames. This gives a reaction barrier that is based on more than 5 ns simulations (31 × 180 000 steps with 1 fs step size). The replica exchange procedures applied here are basically equivalent to averaging the simulations over several

Table 1: Summary of the Activation Energies at Different Runs in the EVB Simulations[a]

	run 1	run 2	run 3	run 4	run 5	run 6	total_map	ave_run	obs[b]
native	12.8	14.1	14.6	16.1	15.9	15.9	14.7	14.9	14.3
L54G	16.6	15.9	14.6	16.1	16.9	14.9	15.5	15.9	16.4
G121V	17.8	18.6	18.4	21.2	19.4	17.4	18.8	18.8	17.3
M42W	14.6	15.4	14.6	14.7	15.3	16.4	15.0	15.2	16.4
M42W-G121V	20.1	21.6	22.6	20.3	20.4	20.9	21.2	21.0	19.7
TmDHFR	22.7	23.7	24.3	23.3	23.6	23.8	23.9	23.6	18.6
water ($\Delta g^{\ddagger}_{\text{cage,DHF}-H^+}$)	19.5	20.3						19.9	20.5[b]
water ($\Delta g^{\ddagger}_{\text{w,DHF}-H^+}$)′								24.4	25.0[b]
water ($\Delta g^{\ddagger}_{\text{w,DHF}}$)′								30.4	31.0[b]

[a] The energies are given in kcal/mol. The simulation of each run involved 31 frames, each of 30 ps. Parallel tempering techniques were used at the end of each run by exchanging the configurations at neighboring frames as described in the text. The FEP/US mapping was done in each individual run and in the total simulations. The first 10% simulation data in each run was excluded in from the FEP/US calculations. [b] See discussion in the section Defining the Catalytic Effect.

different initial conditions plus backward and forward simulations as used in many of our studies (e.g., ref *48*), but the simulations run in parallel and thus reduce the simulation time.

Finally, one may ask about the relationship between the starting structure in the EVB simulations and the actual configurations of the reactant and product. The underlying FEP/US approach is a standard approach whose robustness has been validated extensively. The EVB mapping allows us to reach high-energy regions that cannot be reached simply by forcing the system to move from the reactant and to the product states. This brings the simulated system to the TS in a relatively short simulation time, but the main point is to obtain the correct converging free energy for this transition. The overall simulation used to get the reaction barrier is based on more than 1 ns simulations of systems that previously have been equilibrated for an equally long time. The actual simulation time is in fact significantly longer than 1 ns since we average our results over six runs that started from different initial conditions.

In addition, we would like to reclarify that the reliability of our SCAAS+LRF electrostatic treatment has been established by careful validation studies (see above) and that the trend obtained by our calculations is not sensitive to the H_{ij} used as long as we use the same H_{ij} in all the calculations.

It might be useful to comment here about a recent argument that EVB mapping does not offer any special convergence advantage relative to PMF calculation that changes the solute coordinate (*13*). Unfortunately, the corresponding analysis has not involved any attempt to compare the EVB and the PMF mapping but instead examined the somewhat irrelevant behavior of the energy gap during a PMF mapping. It is hard to realize that a mapping that involves changes of charges and bond lengths (i.e., the EVB) is more effective than the one that only changes bond lengths without performing an actual comparative study. Unfortunately it was assumed in ref *13* that the EVB uses the energy gap as mapping potential. However, the EVB uses the energy gap as the reaction coordinate and for the actual mapping it uses a superposition of the reactant and product potentials (eq 4) that moves the system continuously from the charges and structure of the reactant state to those of the product state, rather than using an artificial constraint on a few bonds. Thus it is important to realize that ref *13* did not examine the EVB mapping approach. One of the main issues is convergence time and hysteresis, and this cannot be examined without actually comparing the two approaches as was done in several of our studies (e.g., refs *49* and *50*).

In the case of charge-transfer reaction, the PMF that uses only the solute coordinates involves significant hysteresis (see ref *51*) while approaches that emphasize the charging coordinates (by using a mapping potential that changes the solute charges) are more reliable. Furthermore, as emphasized in our previous studies (e.g., refs *49* and *50*), the EVB approaches capture the contribution of nonequilibrium effects to the barrier. Finally, the easiest way to see the advantage of the EVB is to consider electron-transfer reactions or reactions when H_{ij} is small (e.g., HT with large donor−acceptor distance). In these cases the PMF approach would be entirely impractical, since we would have to wait an extremely long time until a random solvent fluctuation would lead to change in the solute charges from their values in the reactant state to their values in the product state. On the other hand the EVB mapping does not have to wait for such an improbable event, since it forces the solvent charge to respond to the charges of the mapping potential.

DEFINING THE CATALYTIC EFFECT

Before starting with any quantitative computational or conceptual analysis of the effect of DHFR, it is crucial to have a clear idea about the activation barriers for the reaction of the native enzyme, the mutants, and the thermophile DHFR (TmDHFR) (*52*) as well as the reference reaction in water. Apparently the hydride transfer (HT) reaction is the rate-limiting step at high pH (see ref *53*), and it is possible to extract the pure HT rate constant from measurements at pH = 7.0 (see ref *54*). Thus we used the transition state theory and the pure HT rate constants reported in ref *54*, as well as those estimated from refs *52* and *55*, and extracted the observed activation free energies for the HT step in the enzymes studied in this work (Table 1).

The estimate of the $\Delta g^{\ddagger}$ for the reference reaction in water was much more challenging. To the best of our knowledge, this task has not been accomplished consistently in the countless studies of the reaction of DHFR. The description of the corresponding analysis is somewhat complex (as it must be), and readers who are mainly interested in the mutational effect can skip the rest of this section. At any rate, we started by clarifying that following the detailed discussion in ref *1* we took as a reference reaction that follows the same mechanism as the rate determining step in

the enzyme but occurs in solution (more discussion will be given below). Thus our reference reaction is the hydride transfer (HT) reaction of DHF-H^+. In order to estimate the energetics of this reference reaction we started with the experimental trend reported in ref *56* for a series of related reactions of 2-methyl-5-nitroisoquinolinium ((IQ^+) and a series of NAD(P)H models (*56*) concluded that the corresponding activation barriers are around 19 kcal/mol (see also ref *57*). This reaction is similar but not identical to the reaction of the protonated DHF (DHF-H^+). With this initial estimate we tried to gain more insight about the reaction by performing *ab initio* scans of the energy of the actual reacting system in water, using the B3LYP/6-31+g(d) calculations. Theses calculations (see S4 in the Supporting Information) gave a classical barrier, $\Delta g^{\ddagger}_{w,}$ of about 21 ± 3 kcal/mol for the reaction of Figure 1 (without the charged groups of R and R′) in a solvent cage, where the reactants are in a similar configuration to that in the enzyme. Correcting the calculations to a molar volume gives an extra 2.5 kcal/mol, and then we add our estimate of the contribution from activation entropy of about 3 kcal/mol obtained from related simulation studies (note that this conformational restriction is not used in the EVB simulations). Thus the *ab initio* estimate of $\Delta g^{\ddagger}_{w}$ for the reaction of DHF-H^+ is about 21 + 2.5 + 3 = 26.5 ± 3 kcal/mol (the effect of R and R′ will be considered below). A nuclear quantum mechanical correction of $\Gamma \approx -2$ kcal/mol should also be considered. Obviously our *ab initio* calculations are still preliminary, since their performance has not been examined by reproducing the experimental data set of ref *56* (as should be done in such cases (e.g., ref *58*)), nor have we calculated the difference in barrier between the reaction of DHF-H^+ and IQ^+. At any rate, it seems to us that a reasonable estimate can be obtained by the average between the *ab initio* estimate of the energy (26.5 kcal/mol) of the actual reaction and the observed barrier of a related reaction of IQ^+ (19 kcal/mol). This gives $\Delta g^{\ddagger}_{w}$ of about 23 kcal/mol and $\Delta g^{\ddagger}_{w,quantum}$ of about 21 kcal/mol (where $\Delta g^{\ddagger}_{w,quantum}$ is the barrier that includes the nuclear quantum mechanical (NQM) correction).

Now the above considerations were done for the reference reaction when the reactants are without the charged R and R′. The missing effect involves the *change* in the free energy of moving the system from infinity to the TS, upon turning on the electrostatic interactions between R and R′ (and converting this energy to standard conditions). This term, Δg_{QQ}, can be estimated easily and reliably by using an effective dielectric constant of 30−40 (see ref *23*) and is around 2 kcal/mol. With this correction we have $(\Delta g^{\ddagger}_{w})' = 23 + 2 = 25$ kcal/mol where the ( )′ designates the inclusion of the electrostatic correction. Obviously the above estimate is qualitative, and more systematic studies are needed and some are planned in our group. However, none of our considerations about the reorganization effect in DHFR depend critically on the estimate of $(\Delta g^{\ddagger}_{w})'$.

Some readers might wonder at this point about the relationship between the protonation energy of DHF and the catalytic effect of DHFR. Thus we would like to clarify that the free energy of the (DHF + $H^+ \rightarrow$ DHF-H^+) is given by (*23*)

$$\Delta G_{protonation} \approx 2.3RT(pK_a(\text{DHF-H}^+) - pH) \quad (10)$$

This free energy is about 6 kcal/mol at pH = 7.0 since the pK_a of DHF-H^+ is 2.6 (*59*). However, as has been clarified in many of our works (e.g., ref *1*), we do not consider it as a part of the true catalytic puzzle since our reference state involves the same HT reaction in water and in the protein. Thus, the energy of changing the reaction from the actual reaction in water to the reaction in the enzyme is a well-defined quantity (it is simply given by the above equation). Although understanding the protonation issue is important, it will not change any of our conclusions about the effect of the enzyme on the reaction of the protonated system. In other words the catalytic effect of stabilizing the protonated state by the enzyme is a well-understood effect and is not a part of the long-standing catalytic puzzle, nor does it help to clarify the role of the reorganization energy in the mutant of DHFR and in a solvent cage (which is our main point). We would also like to clarify that the effect of the enzyme on the pK_as of the substrate is around 4 units (±0.3) in all the mutants, and thus it represents more or less a constant term. Nevertheless, the energetics of the reaction that starts with the unprotonated substrate will be also considered in our analysis, where we have $(\Delta g^{\ddagger}_{w,DHF})' = 25 + 6 = 31$ kcal/mol and $(\Delta g^{\ddagger}_{w,DHF-H^+})' = 25$ kcal/mol.

In order to analyze the environmental contributions to the catalytic effect, it is useful to have an effective barrier, $\Delta g^{\ddagger}_{cage}$, for the water reaction when the reacting fragments are already in the same solvent cage. The relationship between $\Delta g^{\ddagger}_{cage}$ and $\Delta g^{\ddagger}_{w}$ corresponds approximately to a free energy difference of 2.5 kcal/mol (this point will be explained in details below). With this correction we get $\Delta g^{\ddagger}_{cage} = 20.5$ kcal/mol. If we consider the NQM, we will have $\Delta g^{\ddagger}_{cage,quantum} \approx 18.5$ kcal/mol. At any rate, we consider in our study the actual $\Delta g^{\ddagger}_{w}$ and would like to clarify that the 2.5 kcal/mol cage correction for the reaction between $\Delta g^{\ddagger}_{cage}$ and $\Delta g^{\ddagger}_{w}$, as well as the ∼2.0 kcal/mol difference between $\Delta g^{\ddagger}_{w}$ and $(\Delta g^{\ddagger}_{w})'$, is a reflection of reliable calculations that allow us to move consistently from $\Delta g^{\ddagger}_{cage}$ to $\Delta g^{\ddagger}_{w}$ and to $(\Delta g^{\ddagger}_{w})'$. Thus, the estimated $(\Delta g^{\ddagger}_{w})'$ corresponds to the actual activation barrier of the reference HT reaction of the deprotonated substrate. This point will be further clarified below. We would also like to clarify that, when we discuss the reorganization energy of the solution reaction, we consider the difference between $(\Delta g^{\ddagger}_{w})'$ and $\Delta g^{\ddagger}_{cage}$ as a part of the work term of eq 7.

Since the cage concept has been frequently misunderstood even by key workers in the field (e.g., ref *60*), where it was incorrectly assumed that the cage constraint fixes the orientation of the reacting fragments in water (see related discussion in ref *61*), it is important to try to reclarify this concept. That is, the rate for a reaction between donor and acceptor ($D^+ + A \rightarrow D + A^+$) is given by

$$\text{rate} = -\Delta[A]/\Delta t = k[D][A] \quad (11)$$

where [D] and [A] are the concentrations of the donor and acceptor molecules (in molar units) and the rate constant, k, is given to a good approximation by (e.g., see ref *23*)

$$k = Fk_BT/h \exp(-\beta\Delta g^{\ddagger}) \quad (12)$$

where F is the transmission factor, k_B is the Boltzmann constant, T is the temperature, h is the Planck constant, and $\beta = 1/k_BT$. Here $\Delta g^{\ddagger}$ is the activation free energy, which is

given for a standard state of 1 M if the concentrations are given in molar units. This does not mean that the reaction has to be done with 1 M concentration, but simply that we have a unified way to express the rate for any concentration. $\Delta g^{\ddagger}/N$ (where N is Avogadro's number) reflects the probability that a system of one donor and one acceptor molecule that is placed at a molar volume ($v_0 = 1660$ Å^3, which corresponds to a sphere with a radius of 7.3 Å) will be at the transition state. Now it is usually impractical to simulate the reaction in a sphere of 7.3 Å, since the simulations require major computational resources. Fortunately, in order to save computer time it is entirely appropriate to divide the probability of reaching the TS into the probability of reaching a reactant state at a cage where two specific donor and acceptor atoms are at a contact distance and the probability of reaching the TS from this configuration. The contact distance is usually defined as being at a cage volume of the size of a water molecule, but any other definition will give the same result (if it is treated consistently as discussed below). This thermodynamic cycle can be written in terms of the corresponding free energies as

$$\Delta g^{\ddagger}_{w} = \Delta g^{\ddagger}_{cage} + k_B T \ln(v_{cage}/v_0)$$
$$(\Delta g^{\ddagger}_{w})' = \Delta g^{\ddagger}_{cage} + k_B T \ln(v_{cage}/v_0) + \Delta g_{QQ} \quad (13)$$

where the index ( )′ indicates that we include the Δg_{QQ} term. The v_{cage} term in the equation can be evaluated rigorously by using a cage constraint, K_{cage}, that corresponds to the given v_{cage}. The free energy of changing K_{cage} to K_0 that corresponds to the molar volume defines exactly the v_{cage} term in eq 13 (see refs *1*, *61*). At any rate, it is sufficient to realize that v_{cage}/v_0 are given approximately by the concentration of water in water (55 M) (see exercise 5.1 in ref *23*). It is important to clarify that our cage treatment does not involve any constraint on the orientation of the reacting fragments (in clear contrast to what is frequently presumed (*60*)). Thus in general (excluding specific convergence problems) the cage effect is a simple addition of about 2.5 kcal/mol. Fortunately in the present case the electrostatic interaction between the tail groups does not contribute to $\Delta g^{\ddagger}_{cage}$ since this contribution is more or less identical in the ground and transition states. Therefore, we can add Δg_{QQ} as a separate contribution as is done in eq 13. Now, although the cage concept provides the clearest way of comparing the enzyme and solution reactions, it can be viewed as a technical issue and there is no reason not to look simply on $\Delta g^{\ddagger}_{w}$. Note, however, that the cage correction is not a part of the catalytic puzzle since it was clearly understood by workers like Jencks and others in the early 1970s (*62*).

The results of the analysis given in this section are summarized in Table 1, together with the corresponding activation barriers for the reaction in the native enzyme and some mutants. In doing so we consider the classical barrier rather than the one with the NQM correction ($\Delta g^{\ddagger}_{quantum}$). This type of approximated treatment is reasonable since the NQM correction is similar in the enzyme and in solution (see discussion in ref *28*). This means that the EVB surface is calibrated on $\Delta g^{\ddagger}_{cage}$ rather than on $\Delta g^{\ddagger}_{cage,quantum}$. Of course, in a more consistent treatment we will have to adjust the classical EVB surface so that $\Delta g^{\ddagger}_{cage,\ quantum}$ would reproduce the corresponding estimate of the "observed"

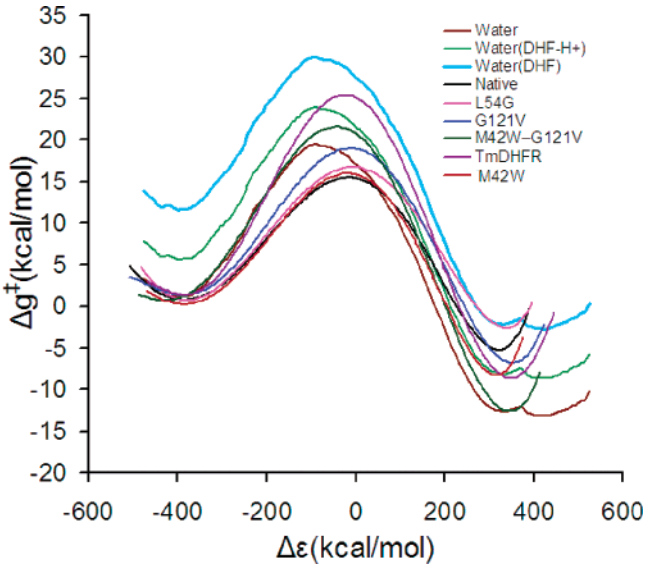

FIGURE 4: The EVB free energy profiles for the hydride transfer reaction of the native DHFR, the mutants, and the reference solution reaction in water. The profiles were obtained by averaging several EVB simulations as described in the text and are given in terms of the EVB reaction coordinate (the $\epsilon_2 - \epsilon_1$ energy gap).

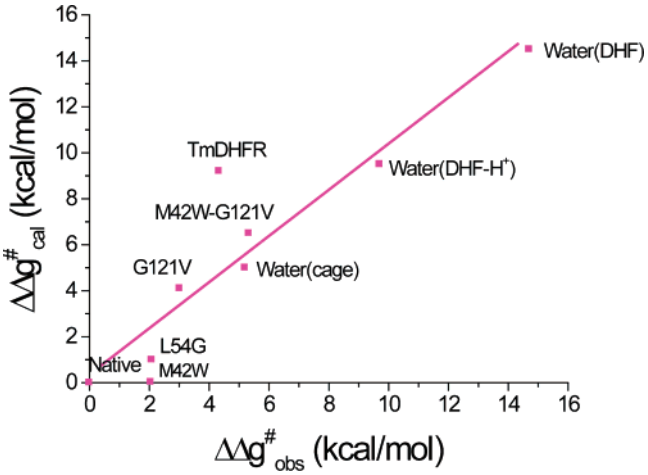

FIGURE 5: The correlation between the calculated and observed changes in activation energies for the reactions of the native DHFR, the designated mutants, the thermophilic TmDHFR, and the reference solution reaction in water. The correlation coefficient (R^2) for the linear regression is 0.6976 without the water data.

$\Delta g^{\ddagger}_{cage}$. This can be done trivially by adjusting H_{12}, but the catalytical effect will stay unchanged.

RESULTS AND DISCUSSION

The first step of our study focused on reproducing the experimentally observed rate constants in the native enzyme, the mutants, and the thermophile DHFR (TmDHFR) (*52*) as well as the reference reaction in water. The calculated activation barriers were evaluated by the EVB−FEP/US procedure, applying extensive averaging over different initial conditions, and the results are summarized in Figure 4 and Table 1. The table also gives the sources of the experimental barriers. The overall agreement between the calculated and observed $\Delta g^{\ddagger}$ is shown in Figure 5. As seen from the figure we reproduced the overall observed trend despite the fact that we are dealing with mutations of distant residues. To the best of our knowledge, this challenging task has not been accomplished by previous studies. For example, ref *63* used

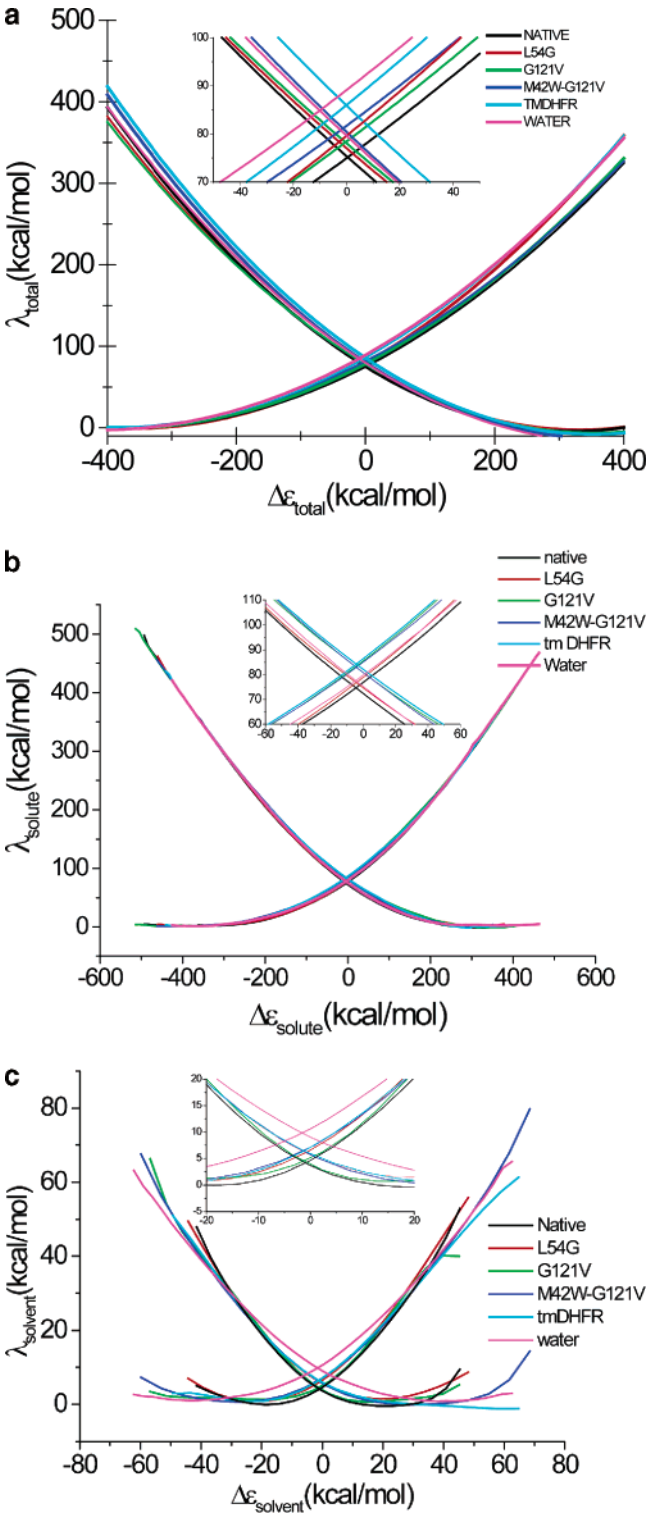

FIGURE 6: The diabatic free energy functional and the solute and solvent contributions for the systems studied in Figure 5. The relevant results are given for the total functional (a), the solute contribution (b), and the solvent contribution (c). The figure displays the functional after shifting the minima to the same heights. The intersection region is magnified in each case.

different off-diagonal terms for the different mutants, while our study used the same EVB potential in all cases. The difference is probably due to our use of very extensive sampling and averaging over different initial conditions.

In the next stage we considered the modified Marcus relationship of eq 7. This treatment required us to evaluate

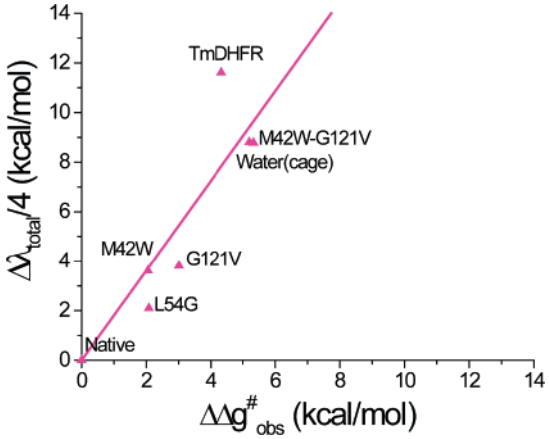

FIGURE 7: Correlation between the changes in the observed activation energies ($\Delta\Delta g^{\ddagger}_{obs}$) of the systems studied in Figure 5 and the calculated changes in the total reorganization energies ($\Delta\Delta\lambda$). The correlation coefficient (R^2) for the linear regression is 0.8062.

the reorganization energy, λ. This could be accomplished by taking the EVB free energy functional (the diabatic free energy curves of eq 6), shifting the minima of the functional to the same heights and taking the resulting height of the intersection (the so-called intrinsic barrier) as $\lambda/4$. The corresponding shifted free energy functionals are shown in Figure 6. However, it was found that the free energy profiles of the diabatic states do not correspond to perfect parabolas and sometimes do not have the same curvature in the reactant and product states. Thus, in order to obtain the most unique description of the reorganization energy, we fitted the profile (up to the intersection point) analytically to perfect parabolas, using the derivation given in the Supporting Information, S3. This fitting is not an arbitrary procedure since it simply extracts the λ that follows the modified Marcus equation (eq 7) in the most general way (note that the diabatic curves were obtained from the simulated energy gap without any arbitrary fitting). Now in the fitting of the simulated parabolas to eq 7, we set the $\bar{w}$ term in eq 7 to zero, since we want to include the effect of the change in the donor−acceptor distance in our λ (a different procedure will also be used below). At any rate, although it was found that the use of calculated ΔG^0 in eq 7 reproduced the calculated $\Delta g^{\ddagger}$ quite accurately, we noted that $\Delta\Delta G^0$ is small relative to λ and explored directly the correlation between the $\Delta\lambda/4$ obtained by the above procedure and the observed $\Delta g^{\ddagger}$. The resulting correlation (Figure 7) seems to be quite encouraging.

The division of the total reorganization energy into solute and solvent contributions did not provide fully additive contributions. This is due to the fact that the solute reorganization energies reflect complicated coupling between stretching and bending modes of the solute and also the donor−acceptor distance. Thus we also explored an alternative representation that used the dependence on the donor and acceptor distance to determine the work term, $\bar{w}$ of eq 7. In general, it is not simple to separate the activation energy into $\bar{w}$ and $\Delta g^{\ddagger}$ in a unique way by considering the experimental dependence of $\Delta g^{\ddagger}$ on ΔG^0 (see discussion in ref *29*). Thus we tried to benefit from the power of the simulation approach and evaluated $\bar{w}$ by calculating the potential of mean force (PMF) for the donor−acceptor distance. The calculated PMFs for the systems studied in this work are described in Figure 8. We view these PMFs

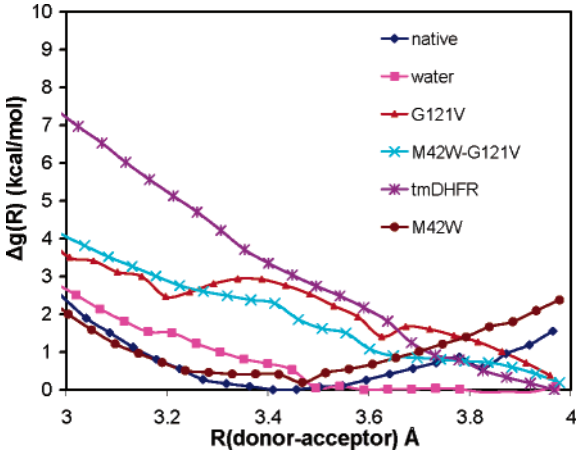

FIGURE 8: The PMF for the donor−acceptor distance for the systems considered in Figure 5. The figure shows that the native enzyme and the aqueous solution system allow the donor and acceptor to reach a similar distance before the hydride transfer process.

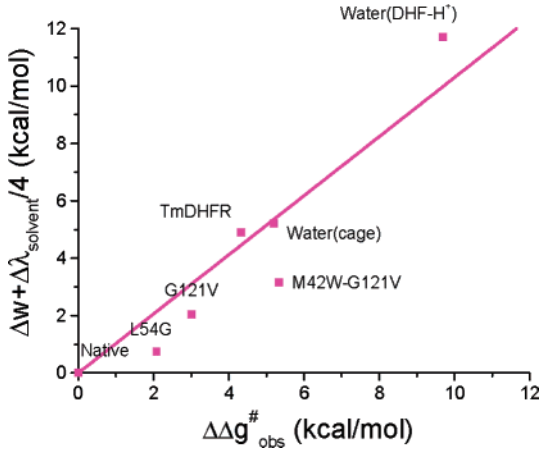

FIGURE 9: The correlation between the changes in the observed activation energy and the calculated activation free energy of eq 14 which gives the barrier in terms of the work term ($\bar{w}$) and the solvent reorganization energy ($\Delta\Delta\lambda_{solvent}$). The correlation coefficient (R^2) for the linear regression is 0.909.

Table 2: The Reorganization Energies and Work Terms for the Native DHFR, Some Mutants, and Other Relevant Systems[a]

	λ_{total}	$\lambda_{solvent}$	λ_{solute}	$\bar{w}$
native	341.6	17.2	324.4	2.2
L54G	329.5	21.1	308.4	2.0
G121V	349.1	20.3	328.8	3.5
M42W-G121V	364.3	22.8	341.5	4.0
TmDHFR	356.4	17.7	338.7	7.1
water[b]	359.8	38.2	321.6	2.6

[a] Energies in kcal/mol and distance in Å. The calculations are done for donor−acceptor distance of 3.0 Å. [b] The contributions from the reaction in water were evaluated while starting the simulations from orientations similar to those of the reactants in the protein but then allowed to sample any point under the weak cage constraint.

as preliminary results due to the well-known convergence problems associated with evaluation of PMF for large displacements (*51*). Thus we consider the work function as the free energy needed to bring the donor acceptor distance from either the minimum or the point with lowest energy (in the range of up to 4 Å) to 3 Å. More systematic studies are in progress in our lab. In addition to these calculations, we also calculated the solvent reorganization energy at 3.0 Å separation, and the results are given in Table 2.

Once the dependence on the donor−acceptor distance is excluded from the calculated solute reorganization energy by evaluating this reorganization energy at a fixed distance, it is reasonable to assume that the rest of the solute reorganization energy is similar in the different systems studied, and to write (assuming that the effect of ΔG_0 is small)

$$\Delta\Delta g^{\ddagger} \cong \Delta\bar{w} + \Delta(\lambda_{solvent}/4) \qquad (14)$$

As seen from Figure 9, we obtain a very encouraging correlation from the use of this relationship.

Another interesting issue is whether coupled modes play a major role in the catalytic effect of DHFR and presumably in other enzymes. Previous studies have provided interesting structural correlations between the motions of different residues (*2*, *3*, *9*). These structural correlations, however, have not provided a complete picture nor established a clear relationship to catalysis. First, a motion of any residue is obviously coupled to those of nearby residues in the same way that the motions of a water molecule are strongly coupled to those of other water molecules during the reference reaction in water. Second, the issue is energy coupling rather than structural coupling. In principle, we could use the approach introduced in ref *64* and explore the energetics of coupling between different residues and between these residues and the TS. However, such a treatment is left to subsequent studies, since the coupled motions of some residues are simply a reflection of the potential surface of the folded protein rather than a catalytic factor. To clarify the effects of the mutations we decomposed the effective free energy surface of the system to its solute and solvent components using eqs 8 and 9. The resulting effective surfaces are shown in Figure 10. As seen from the figure the M42W-G121V mutation leads to a change in the reorganization energy, which is reflected by the increase in the difference between the minima along the solute and solvent coordinate (e.g., ΔQ is 16, 20, and 24 in the native, double mutant, and water, respectively). These changes modify the height of the activation barrier and the reaction paths (shown by arrows in the figures). However, the changes in the surfaces upon mutation can be viewed as an allosteric effect, where changes at a distant site in the protein modify the active site and thus the reaction surface in this site (see the Concluding Remarks section). Apparently, as much as catalysis is concerned, the important issue is the nature of the factors that reduce the barrier and not the possibility that the motion to the transition state involves concerted motions of several residues along the reaction coordinate. In other words, the rate constant is determined by the height of the barrier and not by the shape of the surface up to the barrier (see discussion of the NAC proposal in ref *65*). It is important to recognize that the smaller the motion (the less the reorganization energy), the larger the catalytic effect; this is the significance of having a preorganized active site that involves the smallest possible change upon reaction.

Another useful representation is obtained by plotting the C−H distance (R_{C24-H}) versus the donor−acceptor distance (R_{C24-C9}). This representation, which is related to the common representation of proton transfer surfaces (e.g., ref *66*) is shown schematically in Figure 11. As seen from the figure we have a significant difference between the behaviors

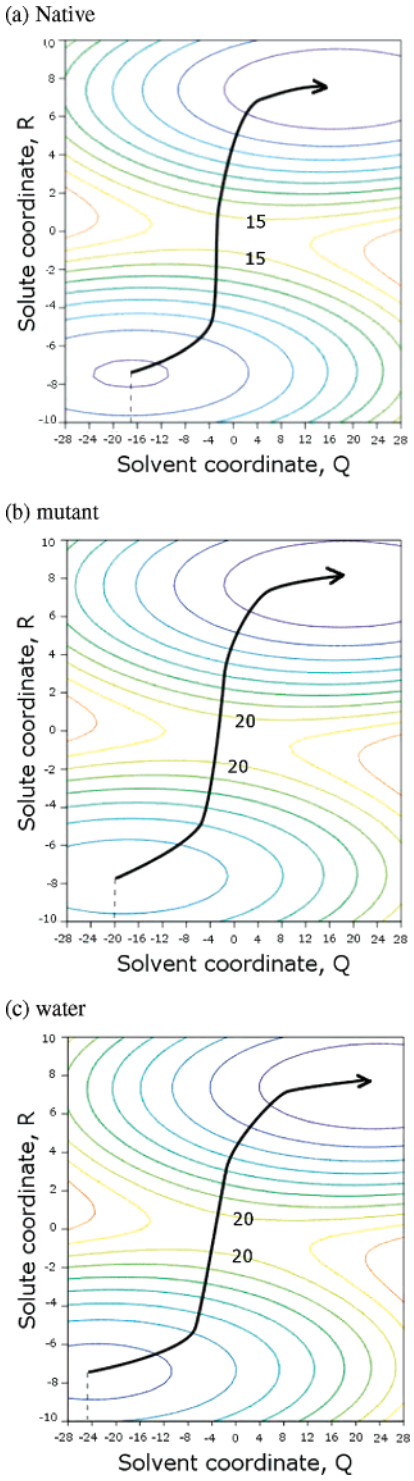

FIGURE 10: The effective free energy surface for the reactions of the native DHFR (a), the M42W-G121V mutant (b), and the reference reaction in water (c). The surfaces are given in terms of the solute and solvent coordinates, which are defined by eq 8 and reflect the solute and solvent reorganization energies (these coordinates are unitless). The difference between the three surfaces can be best appreciated by looking at the values of the solvent coordinate at the minimum of each surface (the minimum changes from about −16 (unitless) in the native enzyme to about −20 (unitless) in water). These changes can be converted to reorganization energies as discussed in the text. The activation energies of the reaction in native protein, M42M-G121V double mutants, and water are 15 kcal/mol, 20 kcal/mol, and 20 kcal/mol, respectively. As can be seen from the figure, the mutation changes the surface in particular along the solvent coordinate and thus changes the path to the TS (shown by arrow).

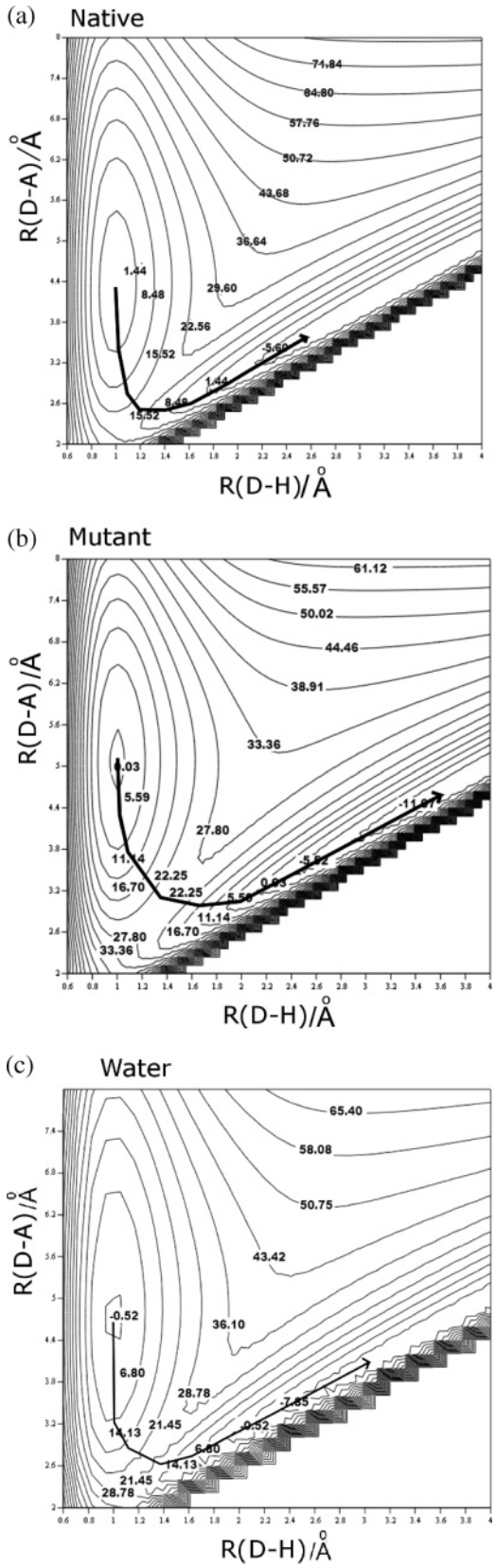

FIGURE 11: The effective free energy surface as a function of R_{C-C} and R_{C-H} for the reactions of the native DHFR (a), the M42W-G121V mutant (b), and the reference reaction in water (c). The surfaces were generated by fitting a simple EVB type potential to the behavior of the actual surface at selected points. The figure illustrates that the donor−acceptor distance at the region where the hydride transfer starts is similar for the enzyme and water reaction and it is larger for the double mutant. The contour lines are given in kcal/mol.

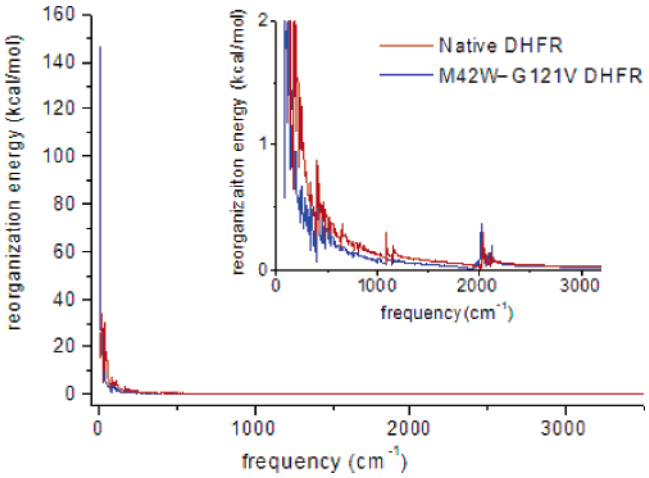

FIGURE 12: Dispersed polaron (DP) distribution analysis of the reaction catalyzed by DHFR and by the M42W-G121V mutant. The DP analysis gives the projection of the modes of the protein−substrate system along the reaction coordinate. The figure captures the low-frequency protein modes which are relevant to the reaction (the C−H stretching modes are only partially captured by this procedure due to their coupling to other motions (see Figure 23.6 in ref *93*)). The main point of the present DP analysis is that it tells us about the coupled modes (which have been the subject of many recent discussions) and demonstrates that the nature of these modes is similar in the native and the mutant enzyme as well in the water reaction (not shown). As discussed elsewhere (e.g., ref *5*), the changes in the heights of the peaks of these modes correspond to the change in their projection on the reaction coordinate and not to dynamical effects. In fact (see eq 9), the overall reorganization energy is given by the integrated intensities of the spectral distributions given in the figure, and obviously the reorganization energy is not a dynamical factor.

at the surface for the native and mutant enzyme. That is, in the native case the donor and acceptor distance reaches about 3.2 Å before the energy starts to increase and the TS occurs with $R_{C-C} \approx 2.6$ Å. On the other hand, in the case of the mutant, the free energy starts to increase fast at about 3.8 Å (see also Figure 10) and the TS occurs with $R_{C-C} \approx 3.0$ Å. The significance of this behavior will be discussed in the next section.

To explore the nature of the reorganization further we also performed a dispersed polaron (spin boson) analysis (*61*, *67*). This is done by evaluating the time dependent energy gap and using the properly weighted Fourier transform of this gap to determine the projection of the protein normal modes along the reaction coordinate. The dispersed polaron (DP) intensities are normalized to reproduce the reorganization energy. The DP analysis is summarized in Figure 12. As seen from this figure, mutations cause changes in the contributions from some of the protein modes. However, as explained elsewhere (e.g., ref *5*), this does not tell us about the magnitude of possible dynamical contributions to catalysis, since the same effects can exist in water and in the protein site. Furthermore, any molecular motion can be approximated by normal modes but, unless the population of such modes is non-Boltzmann, it is not useful to talk on true dynamical effects (see below). Now, while the unlikely possibility of non-Boltzmann effect should be explored, what is undisputed is the fact that the DP spectral distribution reflects the projection of the normal modes of the entire protein plus solvent system on its reaction coordinate (see Figure 2 of ref *68*) rather than a dynamical effect. In other words, the DP spectral distribution reflects the change in the reaction coordinate described in Figure 10. At any rate, we do not wish to focus here on the extremely unlikely possibility that the DP normal modes might involve true coherent dynamical effects, since this will draw the attention from our main point about the reorganization energy. However, we would like to clarify that we are not aware of any study that demonstrated coherence in the protein modes. On the contrary, our analysis of downhill trajectories (e.g., see ref *5*) pointed toward randomization of the energy for motions forward of the TS (see Figure 6 of ref *5*). However, this issue is still open for further research. What is not an open issue is the mathematical fact that the DP gives the quasiharmonic projection of the protein modes on the reaction coordinate and that these projections of the coupled motions sum up to the total reorganization energy rather than to some general new feature as is implied by some workers (see discussion in ref *69*).

CONCLUDING REMARKS

To elucidate the origin of the effect of different mutations on the catalytic reaction of DHFR and other enzymes and to quantify different catalytic proposals, it is essential to have a computational tool that actually reproduces the observed effect of the mutations. The EVB simulations reported in this work reproduced the effects of key mutations in DHFR in a semiquantitative way. Analysis of the mutational effects indicated that they are primarily due to changes in the total reorganization energy or the corresponding change in the "solvent" reorganization energy and the "work term". The semiquantitative correlation between the change in reorganization energy and activation energy provides strong support for our earlier electrostatic proposal (*1*, *70*).

In view of the finding that the effect of distant mutations is associated with the change of the solvent reorganization energy and work function, we have tried to clarify the relationship between this observation and previous studies (*3*, *4*, *11*) that attributed the effects of the mutations to changes in coupled modes. All structural effects in proteins or solutions could be viewed as effects of coupled modes, but doing so does not provide a way of describing the catalytic effect. A more direct description is provided by considering the reaction surface in term of the solute and solvent coordinates. When this is done, it becomes clear that mutations change the reaction coordinate, and that the main reduction in catalysis is associated with the change of the solvent contribution to the reorganization along the reaction coordinate, as well as with the well-understood effect of increasing the donor−acceptor distance that will be discussed below. The reaction in solution has, in fact, a larger change in the displacement of its coupled modes than the reaction in the protein, but this has no direct relationship to catalysis. It is important to emphasize that correlated motions are not a unique feature of enzyme catalysis, because reorganization of the solvent along the reaction path in solution also involves highly correlated motion of many solvent molecules that constitute the overall solvent coordinate (*5*, *71*, *72*). More importantly, the coupling of protein motions to a reaction in an enzyme involves fluctuating electrostatic interactions of the reacting solute with charged or polar residues and bound water molecules. In solution, it involves reorientation of the solvation shells. Clearly, the reaction coordinate in both cases will involve components along the environment (solvent)

coordinate. The real difference is the amplitude of the change in the solvent coordinates during the reaction, which determines the reorganization energy. This amplitude is generally smaller in the enzyme because of preorganization of the active site. This point can be realized by comparing Figure 10a and Figure 10c.

It is important to point out that the effect of distant mutations is not a direct effect but rather the result of perturbations of the protein structure that are propagated to the active site and change $\Delta g^{\ddagger}$. Such long-range coupling of free energy changes has been seen in computer simulations of allosteric effects in hemoglobin (*73*) and the effects of GTPase-activating proteins on the activity of $p21^{ras}$ (*74*). Miller et al. (*75*) have described an impressive experimental demonstration of such an effect in orotidine 5′-phosphate decarboxylase, where removing the ribose 5′-phosphate moiety of the substrate decreases k_{cat}/K_m by more than 12 orders of magnitude. Thus the existence of coupled motions is clearly of great interest in studies of allosteric effects including the control of replication fidelity (*64*). In the case of replication fidelity, it is important to understand the way by which information is transferred from the base binding site to the catalytic site (*64*). However, this understanding does not help in a direct way to understand how enzymes catalyze their reactions relative to the corresponding reactions in water, which is the key requirement for understanding catalysis. The mode coupling effect tells more about the factors used by allosteric enzymes to *destroy* their catalytic machinery than about the factors that native active sites use to catalyze their reactions.

The idea that the effect of the distant mutations are dynamical effects (*7*−*10*) deserves some additional discussion. The most relevant motions must be very fast (in the picosecond range), as is obvious from simulations of downhill trajectories (*76*). Although it is possible to argue that some low-frequency modes of the protein are important in bringing the donor and acceptor close together, the same types of motions are involved in the reference solution reaction. Furthermore, all chemical reactions at room temperature involve thermal motion that leads to reactive events where the probability of reaching the TS is given by the Boltzmann factor of eq 12. This well-known behavior has little to do with the original dynamical proposal (*16*, *17*, *77*, *78*). At present the clearest (although most probably incorrect) dynamical proposal is the idea that the protein (*16*, *17*, *77*, *78*) channels the thermal energy in a coherent (non-Boltzmann) way to motions in the direction of the TS. However, as discussed and demonstrated in many of our works (for review see ref *5*), there is no theoretical or experimental evidence of the involvement of coherent motions in enzyme catalysis, or in any condensed-phase reaction with a barrier of more than few kcal/mol. Similar problems exist with related dynamic proposals (see ref *5*). In this respect it is useful to consider the DP analysis, Figure 12, where we compare the projection of different reaction modes on the reaction coordinate for the native and mutant enzymes. Although there is some change in the distribution of the reactive modes (the modes that have a significant projection on the reaction coordinate), this is not likely to be related to a coherent dynamical effect (see above). The integrated intensity of the DP spectra gives the overall reorganization energy according to eq 9, and this reorganization energy, rather than the exact position of the peaks, determines the activation free energy.

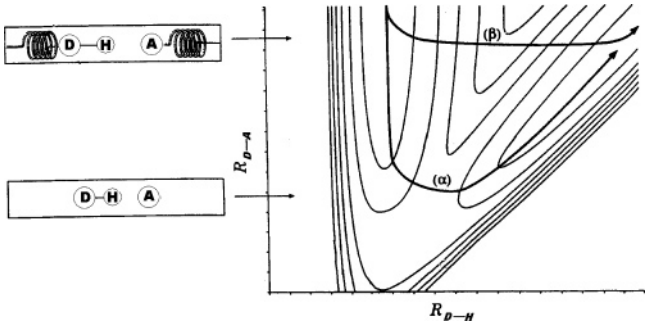

FIGURE 13: A schematic demonstration of the effect of some mutations on the hydride transfer reaction in DHFR. The figure demonstrates that the barrier for hydride transfer increases if the donor−acceptor distance increases (path β). However, in solution and in the native enzyme the transfer occurs through a pathway where the D−A distance is optimal (path α) since the reaction occurs through the α path both in the native enzyme and in solution. Apparently the effect of the mutation on R_{D-A} does not teach us about catalysis (see text). The figure is a modified version of a related figure in ref *23*.

The present work quantifies the idea that some mutations in DHFR increase the distance between the donor and acceptor and thus increase the reaction barrier. This finding is not related to enzyme catalysis, however, but more to the destruction of enzyme catalysis. That is, as was argued in our early analysis (*23*) of the Asp165Glu mutation in triosephosphate isomerase (*79*), the donor and acceptor distance is similar in water and in native enzymes (excluding cases where both the donor and acceptor are charged (*80*)). Even if the distance is slightly larger in water, it costs very little to bring the donor and acceptor in water to the same distance they have in the enzyme. Thus a mutation that holds the donor and acceptor at a large distance reduced the enzyme catalytic effect (e.g., Figure 13), and teaches us how to reduce the catalytic effect but does not tell us how enzymes catalyze their reactions relative to the reference reaction in water. In other words, some mutations are very informative about the key contributions to catalysis (namely, the polar preorganization). This includes mutations of polar groups in the first solvation shell such as oxyanion holes (*81*−*85*) or related electrostatic stabilization effects (*86*). These mutations are very relevant to catalysis since the corresponding preorganized native residues provide an environment which is not available in the reference relation in water (where the solvent has to reorganize during the motion of the reacting system to its TS). On the other hand, mutations that lead to effects that do not exist in water are interesting but not directly relevant to catalysis.

The overall effect of the mutations is summarized schematically in Figure 14. The figure considers the two effects identified in this work: namely, the polar preorganization and the donor−acceptor distance. However, as discussed above, the change in the donor−acceptor distance contributes little to catalysis, and we are left with optimization of the polar preorganization as the truly catalytic effect. This point can be realized better by comparing the reaction in the enzyme to the corresponding reference reaction in water. The general nature of our conclusion can be best appreciated by considering enzymes with much larger catalytic effects than DHFR, where careful analysis attributed most of the catalytic effect to the preorganization effect (*1*).

It has been proposed that the chemical step in DHFR and other enzymes is facilitated by a network of coupled motions

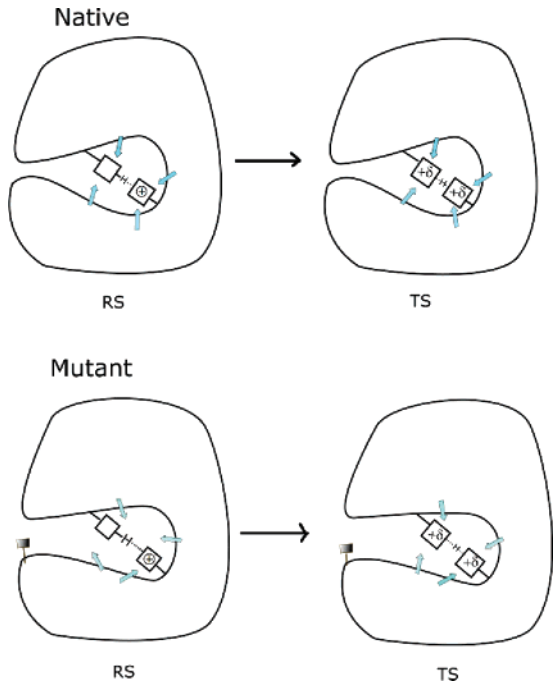

FIGURE 14: A schematic description of the relationship between the changes of preorganization and the donor−acceptor distance to the effect of distant mutations. The native and mutant enzymes are drawn in (a) and (b) respectively. The preorganization effect is illustrated schematically by four dipoles whose orientation is destroyed in the mutant enzyme. The donor−acceptor distance is also increased upon mutation.

that bring the donor and acceptor to the correct distance and orientation and the correct electrostatic environment (*87*). In our opinion, such a new postulate is not required. That is, the minimum of the free energy surface of the reaction in the folded enzyme determines the positions of the donor and acceptor as well as the degree of electrostatic preorganization. The potential surface also determines the nature of the reactive normal modes, which are simply modes with significant projections on the reaction path. The reverse is not true: the reactive motions do not bring the system to the preorganized configuration but take them from the minima in Figure 11 to the TS. In the case of the double mutants, the minimum is not at the preorganized region and the extra motion to the preorganized region is a part of the motion to the TS (this motion does not contribute to catalysis and is simply a part of the process of climbing the overall barrier). Apparently, the folded enzyme establishes the free energy surface for the catalytic reaction, and the motions on this surface simply reflect the Boltzmann probability of finding the system at different points on the surface. The fact that the reaction surface (e.g., Figure 10) is established by interactions between the protein groups and reflects their coupling is well understood (e.g., ref *88*) and does not seem to shed new light on the catalytic effect. What counts is the local polar preorganization in the active site, which is established by the overall folding forces.

Although it is reasonable to describe the motions from the minimum of the reactant state (RS) to the TS in terms of coupled modes, such descriptions provide little new insight about catalysis. Modes that lead from the RS to the TS in lactate dehydrogenase were evaluated and analyzed in a DP study by Yadav et al. (*89*). In that case, the catalysis clearly is determined by the height of the barrier and not by the pathways to this barrier.

Strong coupling between protein residues is a well-known feature of protein folding, which was modeled quiet early (e.g., Levitt and Warshel (*90*)). This coupling obviously determines the final folded structure (or structures) and the path to this structure (e.g., ref *86*). The coupling between the residues also determines the protein normal modes, since as noted above the potential surface determines the normal modes in any system. Again, understanding the folding process is not directly related to catalysis. The relevant issue is the relationship between the folding free energy and catalysis, which appears to be an inverse relationship (*1*, *70*) that works in one direction. Namely, if a mutation reduces catalysis, it should increase the folding energy, but not all mutations that change the folding energy reduce the catalysis. This inverse stability−activity relationship is fully consistent with the relationship between the thermophile enzyme (TmDHFR) and the *Escherichia coli* DHFR (the native enzyme in our study). The different catalytic effects of the thermophilic and mesophilic enzymes are accounted for by the change in reorganization energy, where the native enzyme has a smaller reorganization energy (lowering the activation barrier) and lower stability. It should be noted that the activity−stability relationship is expected when mutations change the active site preorganization since the preorganization requires an investment in folding energy. Thus a mutation that destroys the preorganization should increase the protein stability. However, as stated above, the opposite statement is not always true and mutations that increase the stability do not always change the catalytic effect.

While the long-range effects of mutations in DHFR are very instructive, such effects are relatively minor as far as catalysis is concerned. The catalytic effect of the enzyme is almost entirely due to the local environment. This environment is kept in its correct structure by the overall folding forces of the protein, and the key issue is the degree of correct preorganization in the enzyme−substrate complex. Various perturbations of course can destroy the correct folded structure, and the distant mutations illustrate this. However, it is important to distinguish the origin of the catalytic effect in the correctly folded protein from the factors that lead to this folding.

The finding that the catalytic effect in DHFR is due to reduction of the reorganization energy is not unique to this enzyme. This electrostatic preorganization effect appears to be quite general (e.g., refs *70*, *91*). Even in the case where the catalytic effect is due to a change in the ΔG_0 term in eq 7 (when the product state has a relatively high energy), the catalytic effect results from preorganization of the dipoles that stabilize the charges in the high-energy state (see ref *1*).

ACKNOWLEDGMENT

We gratefully acknowledge the University of Southern California's High Performance Computing and Communications Center for computer time.

SUPPORTING INFORMATION AVAILABLE

(a) Supporting tables S1 and S2, (b) a general treatment for a case with parabolas with different curvature, (c) the full authorship of ref 36, and (d) *ab initio* potential energy surface scan. This material is available free of charge via the Internet at http://pubs.acs.org.

REFERENCES

1. Warshel, A., Sharma, P. K., Kato, M., Xiang, Y., Liu, H., and Olsson, M. H. M. (2006) Electrostatic Basis for Enzyme Catalysis, *Chem. Rev. 106*, 3210−3235.
2. Epstein, D. M., Benkovic, S. J., and Wright, P. E. (1995) Dynamics Of The Dihydrofolate-Reductase Folate Complex−Catalytic Sites And Regions Known To Undergo Conformational Change Exhibit Diverse Dynamical Features, *Biochemistry 34*, 11037−11048.
3. Schnell, J. R., Dyson, H. J., and Wright, P. E. (2004) Structure, dynamics, and catalytic function of dihydrofolate reductase, *Annu. Rev. Biophys. Biomol. Struct. 33*, 119−140.
4. Hammes-Schiffer, S. (2004) Quantum-classical simulation methods for hydrogen transfer in enzymes: a case study of dihydrofolate reductase, *Curr. Opin. Struct. Biol. 14*, 192−201.
5. Olsson, M. H. M., Parson, W. W., and Warshel, A. (2006) Dynamical contributions to enzyme catalysis: Critical tests of a popular hypothesis, *Chem. Rev. 106*, 1737−1756.
6. Wang, L., Tharp, S., Selzer, T., Benkovic, S. J., and Kohen, A. (2006) Effects of a distal mutation on active site chemistry, *Biochemistry 45*, 1383−1392.
7. Miller, G. P., and Benkovic, S. J. (1998) Deletion of a highly motional residue affects formation of the Michaelis complex for Escherichia coli dihydrofolate reductase, *Biochemistry 37*, 6327−6335.
8. Cameron, C. E., and Benkovic, S. J. (1997) Evidence for a functional role of the dynamics of glycine-121 of Escherichia coli dihydrofolate reductase obtained from kinetic analysis of a site-directed mutant, *Biochemistry 36*, 15792−15800.
9. Schnell, J. R., Dyson, H. J., and Wright, P. E. (2004) Effect of cofactor binding and loop conformation on side chain methyl dynamics in dihydrofolate reductase, *Biochemistry 43*, 374−383.
10. Radkiewicz, J. L., and Brooks, C. L. (2000) Protein dynamics in enzymatic catalysis: Exploration of dihydrofolate reductase, *J. Am. Chem. Soc. 122*, 225−231.
11. Rod, T. H., Radkiewicz, J. L., and Brooks, C. L. (2003) Correlated motion and the effect of distal mutations in dihydrofolate reductase, *Proc. Natl. Acad. Sci. U.S.A. 100*, 6980−6985.
12. Watney, J. B., Agarwal, P. K., and Hammes-Schiffer, S. (2003) Effect of mutation on enzyme motion in dihydrofolate reductase, *J. Am. Chem. Soc. 125*, 3745−3750.
13. Garcia-Viloca, M., Truhlar, D. G., and Gao, J. L. (2003) Reaction-path energetics and kinetics of the hydride transfer reaction catalyzed by dihydrofolate reductase, *Biochemistry 42*, 13558−13575.
14. Thorpe, I. F., and Brooks, C. L. (2005) Conformational substates modulate hydride transfer in dihydrofolate reductase, *J. Am. Chem. Soc. 127*, 12997−13006.
15. Boehr, D. D., McElheny, D., Dyson, H. J., and Wright, P. E. (2006) The Dynamic Energy Landscape of Dihydrofolate Reductase Catalysis, *Science 313*, 1638−1642.
16. Gavish, B., and Werber, M. M. (1979) Viscosity-Dependent Structural Fluctuations In Enzyme Catalysis, *Biochemistry 18*, 1269−1275.
17. Careri, G., Fasella, P., and Gratton, E. (1979) Enzyme Dynamics−Statistical Physics Approach. *Annu. Rev. Biophys. Bioeng. 8*, 69−97.
18. Cannon, W. R., Singleton, S. F., and Benkovic, S. J. (1996) A perspective on biological catalysis, *Nat. Struct. Biol. 3*, 821−833.
19. Wang, L., Goodey, N. M., Benkovic, S. J., and Kohen, A. (2006) Coordinated effects of distal mutations on environmentally coupled tunneling in dihydrofolate reductase, *Proc. Natl. Acad. Sci. U.S.A. 103*, 15753−15758.
20. Shurki, A., and Warshel, A. (2003) Structure/function correlations of proteins using MM, QM/MM, and related approaches: Methods, concepts, pitfalls, and current progress, *Adv. Protein Chem. 66*, 249−313.
21. Castillo, R., Andres, J., and Moliner, V. (1999) Catalytic mechanism of dihydrofolate reductase enzyme. A combined quantum-mechanical/molecular-mechanical characterization of transition state structure for the hydride transfer step, *J. Am. Chem. Soc. 121*, 12140−12147.
22. Cummins, P. L., and Gready, J. E. (2003) Computational methods for the study of enzymic reaction mechanisms. II. An overlapping mechanically embedded method for hybrid semi-empirical-QM/MM calculations, *J. Mol. Struct. (THEOCHEM) 632*, 247−257.
23. Warshel, A. (1991) *Computer Modeling of Chemical Reactions in Enzymes and Solutions*, 1997 ed., John Wiley & Sons, New York.
24. Hong, G., Rosta, E., and Warshel, A. (2006) Using the Constrained DFT Approach in Generating Diabatic Surfaces and Off Diagonal Empirical Valence Bond Terms for Modeling Reactions in Condensed Phases, *J. Phys. Chem. B 110*, 19570−19574.
25. Lappe, J., Cave, R. J., Newton, M. D., and Rostov, I. V. (2005) A theoretical investigation of charge transfer in several substituted acridinium ions, *J. Phys. Chem. B 109*, 6610−6619.
26. Hwang, J. K., King, G., Creighton, S., and Warshel, A. (1988) Simulation of Free-Energy Relationships and Dynamics of S_N2 Reactions in Aqueous-Solution, *J. Am. Chem. Soc. 110*, 5297−5311.
27. Marcus, R. A. (1993) Electron-Transfer Reactions In Chemistry−Theory And Experiment (Nobel Lecture), *Angew. Chem., Int. Ed. Engl. 32*, 1111−1121.
28. Warshel, A., Hwang, J. K., and Aqvist, J. (1992) Computer-Simulations of Enzymatic-Reactions−Examination of Linear Free-Energy Relationships and Quantum-Mechanical Corrections in the Initial Proton-Transfer Step of Carbonic-Anhydrase, *Faraday Discuss.* 225−238.
29. Schutz, C. N., and Warshel, A. (2004) Analyzing free energy relationships for proton translocations in enzymes: Carbonic anhydrase revisited, *J. Phys. Chem. B 108*, 2066−2075.
30. Lee, F. S., Chu, Z. T., and Warshel, A. (1993) Microscopic And Semimicroscopic Calculations Of Electrostatic Energies In Proteins By The Polaris And Enzymix Programs, *J. Comput. Chem. 14*, 161−185.
31. King, G., and Warshel, A. (1989) A Surface Constrained All-Atom Solvent Model For Effective Simulations Of Polar Solutions, *J. Chem. Phys. 91*, 3647−3661.
32. Lee, F. S., and Warshel, A. (1992) A Local Reaction Field Method for Fast Evaluation of Long-Range Electrostatic Interactions in Molecular Simulations, *J. Chem. Phys. 97*, 3100−3107.
33. Alden, R. G., Parson, W. W., Chu, Z. T., and Warshel, A. (1995) Calculations of Electrostatic Energies in Photosynthetic Reaction Centers, *J. Am. Chem. Soc. 117*, 12284−12298.
34. Sham, Y. Y., and Warshel, A. (1998) The surface constraint all atom model provides size independent results in calculations of hydration free energies, *J. Chem. Phys. 109*, 7940−7944.
35. Warshel, A., Sharma, P. K., Kato, M., and Parson, W. W. (2006) Modeling electrostatic effects in proteins, *Biochim. Biophys. Acta (BBA)−Proteins Proteomics 1764*, 1647.
36. Frisch, M. J., et al. (2004) in *Gaussian 03, revision C.03*, Gaussian, Inc., Wallingford, CT.
37. Becke, A. D. (1993) A New Mixing of Hartree-Fock and Local Density-Functional Theories, *J. Chem. Phys. 98*, 1372−1377.
38. Lee, C. T., Yang, W. T., and Parr, R. G. (1988) Development of the Colle-Salvetti Correlation-Energy Formula into a Functional of the Electron-Density, *Phys. Rev. B 37*, 785−789.
39. Hehre, W. J., Ditchfie. R, and Pople, J. A. (1972) Self-Consistent Molecular-Orbital Methods.12. Further Extensions of Gaussian-Type Basis Sets for Use in Molecular-Orbital Studies of Organic-Molecules, *J. Chem. Phys. 56*, 2257.
40. Clark, T., Chandrasekhar, J., Spitznagel, G. W., and Schleyer, P. V. (1983) Efficient Diffuse Function-Augmented Basis-Sets for Anion Calculations. 3. The 3-21+G Basis Set for 1st-Row Elements, Li-F, *J. Comput. Chem. 4*, 294−301.
41. Cossi, M., Barone, V., Cammi, R., and Tomasi, J. (1996) Ab initio study of solvated molecules: A new implementation of the polarizable continuum model, *Chem. Phys. Lett. 255*, 327−335.
42. Tomasi, J., Cammi, R., and Mennucci, B. (1999) Medium effects on the properties of chemical systems: An overview of recent formulations in the polarizable continuum model (PCM), *Int. J. Quantum Chem. 75*, 783−803.
43. Howell, E. E., Villafranca, J. E., Warren, M. S., Oatley, S. J., and Kraut, J. (1986) Functional-Role of Aspartic Acid-27 in Dihydrofolate-Reductase Revealed by Mutagenesis, *Science 231*, 1123−1128.
44. Gready, J. E. (1985) Theoretical-Studies On The Activation Of The Pterin Cofactor In The Catalytic Mechanism Of Dihydrofolate-Reductase, *Biochemistry 24*, 4761−4766.
45. Rod, T. H., and Brooks, C. L. (2003) How dihydrofolate reductase facilitates protonation of dihydrofolate, *J. Am. Chem. Soc. 125*, 8718−8719.
46. Geyer, C. J., and Thompson, E. A. (1995) Annealing Markov-Chain Monte-Carlo With Applications To Ancestral Inference, *J. Am. Stat. Assoc. 90*, 909−920.
47. Tesi, M. C., vanRensburg, E. J. J., Orlandini, E., and Whittington, S. G. (1996) Monte Carlo study of the interacting self-avoiding walk model in three dimensions, *J. Stat. Phys. 82*, 155−181.

48. Shurki, A., and Warshel, A. (2004) Why does the Ras switch "break" by oncogenic mutations?, *Proteins 55*, 1−10.
49. Muller, R. P., and Warshel, A. (1995) Ab-Initio Calculations of Free-Energy Barriers for Chemical-Reactions in Solution, *J. Phys. Chem. 99*, 17516−17524.
50. Villa, J., and Warshel, A. (2001) Energetics and dynamics of enzymatic reactions, *J. Phys. Chem. B 105*, 7887−7907.
51. Kato, M., and Warshel, A. (2005) Through the channel and around the channel: Validating and comparing microscopic approaches for the evaluation of free energy profiles for ion penetration through ion channels, *J. Phys. Chem. B 109*, 19516−19522.
52. Maglia, G., Javed, M. H., and Allemann, R. K. (2003) Hydride transfer during catalysis by dihydrofolate reductase from Thermotoga maritima, *Biochem. J. 374*, 529−535.
53. Fierke, C. A., Johnson, K. A., and Benkovic, S. J. (1987) Construction and Evaluation of the Kinetic Scheme Associated with Dihydrofolate-Reductase from Escherichia-Coli, *Biochemistry 26*, 4085−4092.
54. Rajagopalan, P. T. R., Lutz, S., and Benkovic, S. J. (2002) Coupling Interactions of Distal Residues Enhance Dihydrofolate Reductase Catalysis: Mutational Effects on Hydride Transfer Rates, *Biochemistry 41*, 12618−12628.
55. Murphy, D. J., and Benkovic, S. J. (1989) Hydrophobic Interactions Via Mutants Of Escherichia-Coli Dihydrofolate-Reductase—Separation Of Binding And Catalysis, *Biochemistry 28*, 3025−3031.
56. Zhu, X. Q., Liu, Y., Zhao, B. J., and Cheng, J. P. (2001) An old but simple and efficient method to elucidate the oxidation mechanism of NAD(P)H model 1-aryl-1,4-dihydronicotinamides by cations 2-methyl-5-nitroisoquinolium, tropylium, and xanthylium in aqueous solution, *J. Org. Chem. 66*, 370−375.
57. Garcia-Viloca, M., Truhlar, D. G., and Gao, J. (2003) Reaction-Path Energetics and Kinetics of the Hydride Transfer Reaction Catalyzed by Dihydrofolate Reductase, *Biochemistry 42*, 13558−13575.
58. Klahn, M., Rosta, E., and Warshel, A. (2006) *J. Am. Chem. Soc. 128*, 15310−15323.
59. Maharaj, G., Selinsky, B. S., Appleman, J. R., Perlman, M., London, R. E., and Blakley, R. L. (1990) Dissociation-Constants for Dihydrofolic Acid and Dihydrobiopterin and Implications for Mechanistic Models for Dihydrofolate-Reductase, *Biochemistry 29*, 4554−4560.
60. Kollman, P. A., Kuhn, B., and Perakyla, M. (2002) Computational studies of enzyme-catalyzed reactions: Where are we in predicting mechanisms and in understanding the nature of enzyme catalysis?, *J. Phys. Chem. B 106*, 1537−1542.
61. Warshel, A., and Parson, W. W. (2001) Dynamics of biochemical and biophysical reactions: insight from computer simulations, *Q. Rev. Biophys. 34*, 563−679.
62. Jencks, W. P. (1969) *Catalysis in chemistry and enzymology*, McGraw-Hill, New York.
63. Wong, K. F., Selzer, T., Benkovic, S. J., and Hammes-Schiffer, S. (2005) Impact of distal mutations on the network of coupled motions correlated to hydride transfer in dihydrofolate reductase, *Proc. Natl. Acad. Sci. U.S.A. 102*, 6807−6812.
64. Xiang, Y., Oelschlaeger, P., Florian, J., Goodman, M. F., and Warshel, A. (2006) Simulating the Effect of DNA Polymerase Mutations on Transition-State Energetics and Fidelity: Evaluating Amino Acid Group Contribution and Allosteric Coupling for Ionized Residues in Human Pol b, *Biochemistry 45*, 7036−7048.
65. Strajbl, M., Shurki, A., Kato, M., and Warshel, A. (2003) Apparent NAC effect in chorismate mutase reflects electrostatic transition state stabilization, *J. Am. Chem. Soc. 125*, 10228−10237.
66. Truhlar, D. G., Gao, J. L., Garcia-Viloca, M., Alhambra, C., Corchado, J., Sanchez, M. L., and Poulsen, T. D. (2004) Ensemble-averaged variational transition state theory with optimized multidimensional tunneling for enzyme kinetics and other condensed-phase reactions, *Int. J. Quantum Chem. 100*, 1136−1152.
67. Hwang, J. K., and Warshel, A. (1997) On the relationship between the dispersed polaron and spin-boson models, *Chem. Phys. Lett. 271*, 223−225.
68. Warshel, A., Chu, Z. T., and Parson, W. W. (1989) Dispersed Polaron Simulations of Electron-Transfer in Photosynthetic Reaction Centers, *Science 246*, 112−116.
69. Warshel, A., and Villa-Freixa, J. (2003) Comment on "Effect of active site mutation Phe93 → Trp in the horse liver alcohol dehydrogenase enzyme on catalysis: A molecular dynamics study", *J. Phys. Chem. B 107*, 12370−12371.
70. Warshel, A. (1978) Charge Stabilization Mechanism in Visual and Purple Membrane Pigments, *Proc. Natl. Acad. Sci. U.S.A. 75*, 2558−2562.
71. Warshel, A. (1984) Dynamics Of Enzymatic-Reactions, *Proc. Natl. Acad. Sci. U.S.A. 81*, 444−448.
72. Hwang, J. K., Chu, Z. T., Yadav, A., and Warshel, A. (1991) Simulations Of Quantum-Mechanical Corrections For Rate Constants Of Hydride-Transfer Reactions In Enzymes And Solutions, *J. Phys. Chem. 95*, 8445−8448.
73. Warshel, A., and Weiss, R. M. (1981) Energetics Of Heme-Protein Interactions In Hemoglobin, *J. Am. Chem. Soc. 103*, 446−451.
74. Glennon, T. M., Villa, J., and Warshel, A. (2000) How does GAP catalyze the GTPase reaction of Ras? A computer simulation study, *Biochemistry 39*, 9641−9651.
75. Miller, B. G., Snider, M. J., Short, S. A., and Wolfenden, R. (2000) Contribution of Enzyme-Phosphoribosyl Contacts to Catalysis by Orotidine 5′-Phosphate Decarboxylase, *Biochemistry 39*, 8113−8118.
76. Olsson, M. H. M., and Warshel, A. (2004) Solute Solvent Dynamics and Energetics in Enzyme Catalysis: The S_N2 Reaction of Dehalogenase as a General Benchmark, *J. Am. Chem. Soc. 126*, 15167−15179.
77. McCammon, J. A., Wolynes, P. G., and Karplus, M. (1979) *Biochemistry 18*, 927.
78. Karplus, M., and McCammon, J. A. (1983) *Annu. Rev. Biochem.* 163−180.
79. Raines, R. T., Sutton, E. L., Straus, D. R., Gilbert, W., and Knowles, J. R. (1986) Reaction Energetics of a Mutant Triosephosphate Isomerase in Which the Active-Site Glutamate Has Been Changed to Aspartate, *Biochemistry 25*, 7142−7154.
80. Strajbl, M., Shurki, A., Kato, M., and Warshel, A. (2003) Apparent NAC Effect in Chorismate Mutase Reflects Electrostatic Transition State Stabilization, *J. Am. Chem. Soc. 125*, 10228−10237.
81. Wells, J. A., Cunningham, B. C., Graycar, T. P., and Estell, D. A. (1986) Importance of Hydrogen-Bond Formation in Stabilizing the Transition-State of Subtilisin, *Philos. Trans. R. Soc. London A 317*, 415−423.
82. Carter, P., and Wells, J. A. (1988) Dissecting the Catalytic Triad of a Serine Protease, *Nature 332*, 564−568.
83. Warshel, A., Sussman, F., and Hwang, J. K. (1988) Evaluation of Catalytic Free-Energies in Genetically Modified Proteins, *J. Mol. Biol. 201*, 139−159.
84. Kuliopulos, A., Talalay, P., and Mildvan, A. S. (1990) Fluorescence and NMR Properties of the Sole Tyrosine (Tyr-14) in a Double Mutant of Delta-5-3-Ketosteroid Isomerase (Ksi), *Biochemistry 29*, 2197−2198.
85. Feierberg, I., and Aqvist, J. (2002) The catalytic power of ketosteroid isomerase investigated by computer simulation, *Biochemistry 41*, 15728−15735.
86. Fersht, A. (1999) *Structure and mechanism in protein science: a guide to enzyme catalysis and protein folding*, W. H. Freeman, New York.
87. Hammes-Schiffer, S., and Benkovic, S. J. (2006) Relating protein motion to catalysis, *Annu. Rev. Biochem. 75*, 519−541.
88. Glennon, T. M., and Warshel, A. (1998) Energetics of the Catalytic Reaction of Ribonuclease A: A Computational Study of Alternative Mechanisms, *J. Am. Chem. Soc. 120*, 10234−10247.
89. Yadav, A., Jackson, R. M., Holbrook, J. J., and Warshel, A. (1991) Role of Solvent Reorganization Energies in the Catalytic Activity of Enzymes, *J. Am. Chem. Soc. 113*, 4800−4805.
90. Levitt, M., and Warshel, A. (1975) Computer-Simulation of Protein Folding, *Nature 253*, 694−698.
91. Bjelic, S., and Aqvist, J. (2006) Catalysis and linear free energy relationships in aspartic proteases, *Biochemistry 45*, 7709−7723.
92. Humphrey, W., Dalke, A., and Schulten, K. (1996) VMD: Visual molecular dynamics, *J. Mol. Graphics 14*, 33.
93. Kohen, A., and Limbarch, H. (2006) *Isotopic effects in chemistry and biology*, Taylor & Francis Group, LLC, Boca Raton.

BI700201W